18

Optoelectronic Tweezers for the Manipulation of Cells, Microparticles, and Nanoparticles

Aaron T. Ohta[1], Pei-Yu Chiou[2], Arash Jamshidi[3], Hsan-Yin Hsu[3], Justin K. Valley[3], Steven L. Neale[3], and Ming C. Wu[3]
[1]*University of Hawaii at Manoa*
[2]*University of California, Los Angeles*
[3]*University of California, Berkeley*
USA

1. Introduction

Micro- and nanoparticle manipulation capabilities can benefit researchers in a wide variety of fields, from biological research to semiconductor physics. Optoelectronic tweezers (OET) is a novel technique that complements existing manipulation technologies. OET provides optically-controlled manipulation at the single-particle level. It is a dynamic, reconfigurable, minimally-invasive tool capable of massively parallel manipulation. In this chapter, the operating principle of OET will be explained, along with device design considerations and operational regimes. The capabilities of OET will be showcased in the context of applications in biological cell handling and micro- and nanoparticle assembly.

1.1 Methods of micro- and nanoparticle manipulation

Many research fields benefit from the ability to address particles in the micro- and nanoscale regimes. For example, biologists have traditionally studied cell behavior by observing the bulk response of a population of cells. However, it can be desirable to observe the behavior of a single cell. This information is useful for studying phenomena such as cell-cell interactions, cell signaling pathways, mutations or genetic damage among a population, or the differentiation of stem cells. In addition, the response of a single cell can be observed, instead of the average response of an entire population. Certain cells in a homogeneous population may exhibit behavior that deviates from the average response; single-cell observation may provide more insight into the cause of the deviant response. Thus, studies at the single-cell level are greatly facilitated by the ability to manipulate individual cells.

Non-biological particle manipulation is also of interest for engineering fields. Nanostructures that exhibit quantum-mechanical behavior are interesting to researchers studying nanoscale physics, or to engineers that are exploiting the unique properties of nanomaterials for improved devices. However, an obstacle to nanostructure research is the difficulty in addressing and assembling these extremely small particles.

Micro- and nanoscale manipulation can be achieved with a variety of forces, including mechanical, magnetic, fluidic, optical, and electrokinetic forces. These forces are controlled

Source: Recent Optical and Photonic Technologies, Book edited by: Ki Young Kim,
ISBN 978-953-7619-71-8, pp. 450, January 2010, INTECH, Croatia, downloaded from SCIYO.COM

by a wide variety of devices. Perhaps the most intuitive devices are the mechanical manipulators, such as microgrippers for cells (Kim et al., 1992; Chronis & Lee, 2005) or atomic-force microscope tips for nanoparticle positioning (Avouris et al., 1999). However, non-contact methods are often preferred by biologists. In addition, it is difficult to scale up the number of mechanical manipulators in order to increase the parallel manipulation capabilities of the device.

Magnetic forces are not invasive, but this technique requires particles to be attached to magnetic beads, unless the particle has an intrinsic magnetic response. This limits the type of particles that can be manipulated by magnetic fields (Gosse & Croquette, 2002). Furthermore, tag-free protocols that do not require attaching cells to magnetic beads or other particles are more attractive to most biologists.

Microfluidic devices are another non-contact method of cellular manipulation (West et al., 2008). However, it is difficult to target a specific single cell in current microfluidic devices, although they are suitable for sorting heterogeneous cell populations.

Optical tweezers provides dynamic, flexible manipulation of specific single cells. Optical tweezers uses the gradient force of light to trap particles using a highly-focused laser beam (Ashkin et al., 1986), and has been used in many research applications, such as measuring cell motility (Maier et al., 2004), sorting colloidal particles (MacDonald et al., 2003), sorting cells (Paterson et al., 2005), and trapping and assembling nanowires (Pauzauskie et al., 2006). In addition, the basic single-beam optical trap has been extended to multiple traps from a single laser source using holographic imaging (Grier, 2003), evanescent-wave traps (Garces-Chavez et al., 2005), and plasmonic-enhanced traps (Miao & Lin, 2007; Grigorenko, et al., 2008).

The basic single-beam optical tweezers trap is formed when a laser beam is highly focused. Near the focal point, lateral trapping forces are created due to the gradient force of the light. Along the axial direction of the laser, a force due to radiation pressure also exists. Thus, the trap is only stable in three dimensions if the axial gradient force near the focal point is stronger than the forces from radiation pressure. A typical optical trap requires an intensity of approximately 10^7 mW/cm^2, which requires high-power lasers, and can damage some types of particles, including cells (Konig et al., 1996, Neuman et al., 1999; Mohanty et al., 2002). In addition, the generation of sufficient optical gradients requires high numerical aperture objective lenses to focus the laser; this results in a limited optical manipulation area, reducing parallel manipulation capabilities, especially for larger microscale particles such as cells.

1.2 Dielectrophoresis

Electrokinetic forces are capable of non-contact, non-invasive parallel manipulation. These forces include electrophoresis and dielectrophoresis. Electrophoresis is the movement of charged particles within an electric field, and is commonly used to separate DNA molecules by size. Dielectrophoretic manipulation is more attractive, as it is capable of acting on neutral particles as well as charged particles.

Dielectrophoresis (DEP) is the electrical analog of optical tweezers. This phenomena relies on the gradient force of an electric field rather than an optical field (Pohl, 1958). The induced dipole of a particle experiences a force due to the electric field gradient, resulting in dielectrophoretic force. Dielectrophoresis acts on a variety of particles, including non-conductive particles, conductive particles, particles that have a net electric charge, or particles that are charge-neutral. DEP forces are also capable of trapping nanoparticles

(Muller et al., 1996) through the use of microfabricated electrodes. DEP-based devices have been demonstrated in applications ranging from cell trapping and cell sorting (Gascoyne et al., 1997; Cheng et al., 1998; Huang et al., 2003; Gascoyne et al., 2004; Pethig et al., 2003) to carbon nanotube separation (Krupke et al., 2003) and nanowire assembly (Evoy et al., 2004). Electrode-based DEP devices have parallel manipulation capabilities, but the trapping patterns are fixed, and it is difficult to isolate a single particle of interest. This capability can be achieved by creating dynamic DEP cages via CMOS control (Fuchs et al., 2006). However, this device is limited by the pitch of the CMOS circuitry, and is currently limited to microscale manipulation.

2. Optoelectronic Tweezers (OET)

Optoelectronic tweezers (OET) enables the optically-controlled, parallel manipulation of single micro- and nanoscale particles. This device, first developed by Wu, et al. (Chiou et al., 2005) integrates the flexibility and control of optical manipulation with the parallel manipulation and sorting capabilities of dielectrophoresis, resulting in optically-induced dielectrophoresis. The OET device uses a photosensitive surface to allow an optical pattern to control the electric field landscape within an OET device. The resulting non-uniform electric field then generates a DEP force on particles. Unlike optical tweezers, the optical energy is not directly used for trapping, so much lower optical intensities can be used: 10 to 1000 mW/cm^2. These optical intensities can be achieved by a computer projector or an LED, allowing the creation of complex optical manipulation patterns (Ohta et al., 2007c). In addition, the optical gradient force is no longer required, relaxing the focusing requirements and allowing the use of low numerical aperture lenses. As a result, the effective manipulation area of OET can be over 500 times larger than that of a typical optical tweezers setup. Furthermore, since the manipulation patterns are controlled optically, OET retains the flexibility and dynamic control enjoyed by optical tweezers. Unlike electrode-based DEP, OET is capable of trapping a specific single particle from a larger population. In addition to the advantages presented by optically-controlled manipulation, OET also retains the properties of DEP. Different cells experience varying DEP forces, allowing the separation of cells based on the DEP response.

OET manipulation has been demonstrated on a variety of microparticles, including polystyrene beads (Chiou et al., 2005; Ohta et al., 2007a), *E. coli* bacteria (Chiou et al., 2004), red and white blood cells (Ohta et al., 2007c; Hwang et al., 2008a), HeLa cells (Ohta et al., 2007a; Neale et al., 2009a), Jurkat cells (Ohta et al., 2007a), yeast cells (Lu et al., 2005), and protozoa (Choi et al., 2008). In addition, OET is capable of manipulating semiconducting and metallic nanowires (Jamshidi et al., 2008).

The basic OET device consists of two electrodes (Figure 1a). The upper transparent electrode consists of a 100-nm-thick layer of indium tin oxide (ITO), a transparent conductive material, on a glass substrate. The lower photosensitive electrode typically consists of featureless layers of ITO and intrinsic amorphous silicon (a-Si) on a glass substrate. The two electrodes are separated by spacers, creating a chamber between the electrodes that is typically 100 μm in height. An aqueous solution containing the cells or particles under manipulation is introduced into the chamber between the electrodes. An electric field is created in the device by applying an ac bias across the top and bottom electrodes.

The OET device is placed under a microscope for observation of the particles under manipulation. Optical patterns are focused onto the photosensitive surface, typically using

a microscope objective lens. The optical source is flexible. A low-power laser can be used, or an incoherent light source such as a halogen or mercury lamp, or a light-emitting diode (LED). Optical patterns are created using spatial light modulators, such as Texas Instrument's digital micromirror device (DMD), a MEMS mirror array, or Hamamatsu's liquid-crystal-based spatial light modulator. The optical source and the optical patterning system can also be integrated by focusing the output of a computer projector (Ohta et al., 2007c) or LCD display (Choi et al., 2007; Hwang et al., 2008a) onto the OET device.

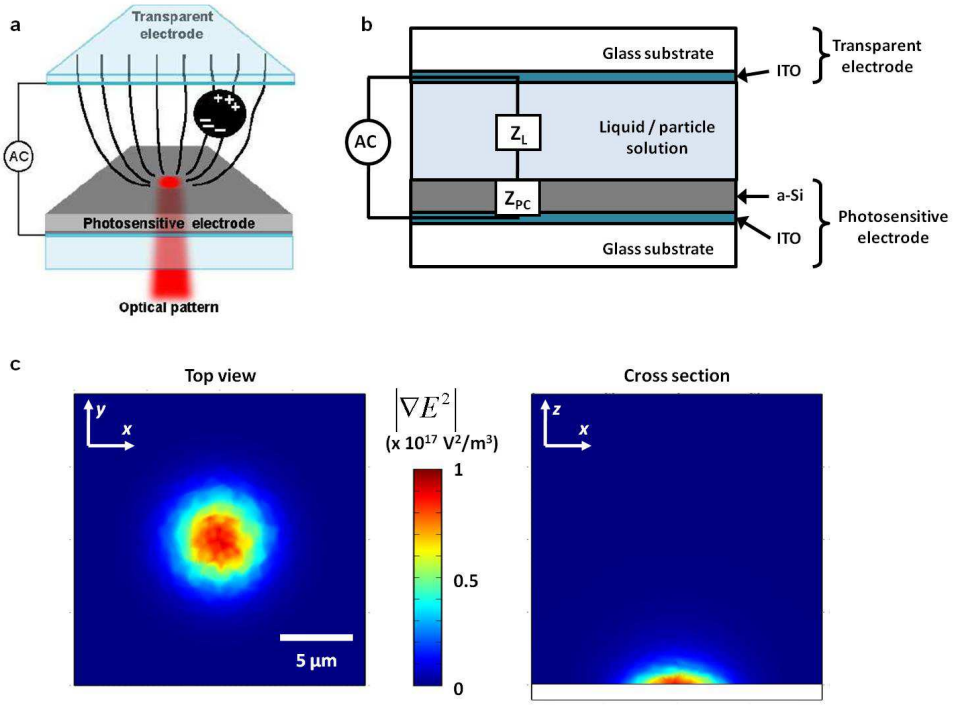

Fig. 1. The optoelectronic tweezers (OET) device. (a) Physical structure of the OET device, consisting of a transparent electrode and a photosensitive electrode. The illuminated areas create optically-defined electrodes on the photosensitive surface, creating electric field gradients that generate optically induced dielectrophoretic force. (b) Simplified equivalent circuit model. (c) Simulation of the gradient of the square of the electric field in the liquid layer of an OET device, which is proportional to the induced dielectrophoretic force. The areas of highest gradients correspond to a spot illuminated by an optical source.

2.1 Operating principle

The OET device relies on optically-induced dielectrophoresis to impart a force on the particles under manipulation. The dielectrophoretic force is controlled by optical patterns that are projected on the photosensitive surface of the device.

Amorphous silicon, the material used in the photosensitive electrodes of OET, has its conductivity modulated by the intensity of the light that is absorbed in the material. Under ambient lighting conditions, the a-Si film has a low conductivity. However, when

illuminated with light, photogenerated charge carriers are produced in the a-Si. As a result, the conductivity of the a-Si layer increases by a few orders of magnitude. The a-Si layer thus has two states; a low-conductivity dark state, and high-conductivity illuminated state. These two states allow the a-Si layer to act as an optically-controlled and optically-defined electrode. The resolution of the optically-defined electrode has been shown to be a function of the size and intensity of the optical patterns (Ohta et al., 2007c; Neale et al., 2007).

The importance of the a-Si photoconductive layer can be seen by modeling the OET devices with a simplified equivalent circuit model (Figure 1b). In the dark state, the impedance of the a-Si, Z_{PC}, is larger than the impedance of the liquid layer, Z_L. Thus, in areas with no illumination, most of the applied ac voltage drops across the high impedance of the a-Si layer. However, in the illuminated areas, Z_{PC} becomes significantly lower, allowing a significant voltage drop to occur in the liquid layer. In this manner, an electric field gradient is set up between the illuminated and dark areas in the OET device (Figure 1c).

The electric field gradients in the OET and LOET devices result in an optically-induced dielectrophoretic force. This DEP force results from the interaction of a non-uniform electric field and the induced dipole of a particle within the electric field. The forces at each at end of the particle's dipole are unequal due to the non-uniform field, resulting in a net force. This force can be described by the following equation:

$$F = \overline{p} \cdot \nabla \overline{E} \tag{1}$$

where $\overline{p}$ is the dipole moment of the particle, and $\overline{E}$ is the first term of the Taylor series expansion of the electric field (Jones, 1995). If the particle is a homogeneous dielectric sphere (e.g. a polystyrene bead), then the time-averaged DEP force reduces to:

$$F_{DEP} = F_{OET} = 2\pi r^3 \varepsilon_m \,\mathrm{Re}[K(\omega)] \nabla E_{rms}^2 \tag{2}$$

where r is the particle radius, ε_m is the permittivity of the medium surrounding the particle, E_{rms} is the root-mean-square electric field strength, and Re[$K(\omega)$] is the real part of the Clausius-Mossotti factor, given by:

$$K(\omega) = \frac{\varepsilon_p^* - \varepsilon_m^*}{\varepsilon_p^* + 2\varepsilon_m^*}, \varepsilon_p^* = \varepsilon_p - j\frac{\sigma_p}{\omega}, \varepsilon_m^* = \varepsilon_m - j\frac{\sigma_m}{\omega} \tag{3}$$

where ε is the permittivity of the particle or medium (denoted by a subscript p or m), σ is the conductivity of the particle or medium, and ω is the angular frequency of the electric field (Jones, 1995). The magnitude of Re[$K(\omega)$] varies with frequency, resulting in a frequency-dependence of the dielectrophoretic force. Positive values of Re[$K(\omega)$] result in particle attraction to electric field maxima (positive DEP, referred to here as positive OET). For negative values of Re[$K(\omega)$], particles are repelled from field maxima (negative DEP, referred to here as negative OET). Applying an AC electric field thus allows the tuning of the type of DEP force induced on a particle, as well as negating any electrophoretic effects, or particle movement due to its surface charge.

If the particle under manipulation is non-homogeneous, like biological cells, Equation 3 must be modified. A single-shell model is typically used to determine the frequency-dependent Clausius-Mossotti factor for mammalian cells. The permittivity and conductivity of the cell membrane and interior are used to determine an effective complex permittivity that can then be used in Equation 3. This effective permittivity is given by:

$$\varepsilon_p^* = C_{mem}^* \frac{3r\varepsilon_{\text{int}}^*}{3\varepsilon_{\text{int}}^* + 3C_{mem}^* r} \tag{4}$$

where $\varepsilon_{\text{int}}^*$ is the complex internal conductivity of the cell, assuming that the thickness of the cell membrane, d, is much less than the radius of the cell interior, r (Gascoyne et al., 1997). The membrane capacitance, C_{mem}^*, is given by:

$$C_{mem}^* = \frac{\varepsilon_{mem}}{d} - \frac{j\sigma_{mem}}{d} \tag{5}$$

Many cell types are uniquely distinguishable by the real part of the Clausius-Mossotti factor. This enables the separation of different cell types using DEP force.

2.2 Operational modes of Optoelectronic Tweezers

In addition to optically-induced dielectrophoresis, several other effects can occur in the OET device (Valley et al., 2008). Most of these are undesirable parasitic effects, but some of these operational modes can be used to obtain expanded functionality in the OET device.

One of the parasitic effects in the OET device is electrolysis: the breakdown of water molecules into hydrogen and oxygen gas due to an electric current. This is undesirable, as the bubble formation can rupture cell membranes and interfere with OET operation. In addition, if the bubble formation process is violent enough, the a-Si film can crack, or pinholes can form. Electrolysis is more prevalent when using electric fields at a frequency of 1 kHz or less.

Another undesirable effect is electrothermal heating, as elevated temperatures can cause cell death or even boiling of the liquid media. The electrothermal heating is caused by phonon generation in the a-Si layer or joule heating in the a-Si and liquid layers. As a result, gradients in the electrical conductivity and permittivity of the liquid media arise, resulting in a liquid flow. However, these effects are only significant under high optical intensities (greater than 100 W/cm^2).

Light-induced AC electroosmosis (LACE) is another operational regime of the OET device, typically occurring at low bias frequencies of approximately 1 kHz. Unlike the other effects, LACE is a useful operating mode of the OET device. The LACE effect is an optically-patterned control of fluid flow in the OET device. The optical patterns control the zeta potential at the liquid-photoconductor interface as well as the electric field profile, creating localized fluid flows surrounding the illuminated areas. The LACE flows have been used to trap polystyrene beads with diameters of 2 μm down to 50 nm, λ-phage DNA molecules, and quantum dots (Chiou et al., 2008), and to separate 1-μm-diameter beads from 6-μm-diameter beads (Hwang & Park, 2009a).

A figure of merit has been developed to quantify the contribution of these other effects relative to the strength of the optically-induced DEP force. This is expressed as a ratio, β:

$$\beta = \frac{X_{DEP}}{X_{DEP} + X_{EXT} + \left\langle X_{BROWNIAN} \right\rangle} \tag{6}$$

where X_{DEP}, X_{EXT}, and $\left\langle X_{BROWNIAN} \right\rangle$ represent the distance a particle travels in 1 s due to optically-induced DEP, all other external forces, and Brownian motion, respectively (Valley et al., 2008). If β is averaged over an area, a new figure of merit is obtained:

$$B = \frac{1}{A}\int_A \beta dxdy, \qquad x \in [-r, r], y \in [0, d] \tag{7}$$

where r is the maximum radius from the center of the optical pattern that particle perturbation is expected, d is the thickness of the liquid layer, and A is the area of integration, where $A = 2rd$. Thus, B represents the percentage of particle perturbation in the OET device due to optically-induced DEP. For applied bias frequencies of greater than 50 kHz and optical intensities of less than 100 W/cm^2 (typical OET operating parameters), optically-induced DEP is indeed the dominant force (Figure 2).

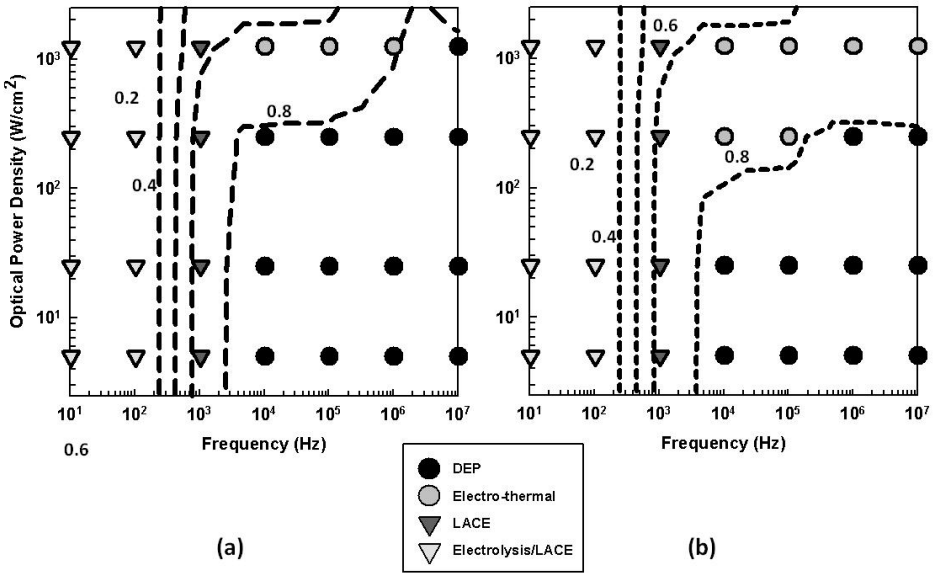

Fig. 2. Dominant effects in the OET device. Theoretical simulations are shown as dashed lines, and empirically-determined effects are shown as data points. The liquid solution has a conductivity of 1 mS/m. The applied voltage is at a frequency of 100 kHz, with amplitudes of (a) 20 Vpp and (b) 10 Vpp. Reprinted with permissions from Valley et al., 2008. Copyright 2008, IEEE.

2.3 Other Optoelectronic Tweezers devices

Thus far, the standard configuration of the OET device has been discussed. In addition to this standard configuration, there are other variants on the OET device, which are described here.

One modification is the substitution of alternate materials for the amorphous silicon photosensitive electrode. The amorphous silicon is deposited using plasma-enhanced vapor deposition (PECVD). If PECVD equipment is unavailable or infeasible, an alternative is to use photosensitive polymers in lieu of amorphous silicon. One suitable polymer blend material is a mixture of regioregular poly (3-hexylthiophene) (rr-P3HT) and phenyl-C61-butyric acid methyl ester (PCBM), forming a P3HT/PCBM blend, which is also used in

plastic solar cells (Padinger et al., 2003). OET devices fabricated with P3HT/PCBM polymer films in place of amorphous silicon have similar functionality to standard OET devices (Wang et al., 2009).

Another alternate photosensitive material is cadmium sulphide (CdS), which is another photoconductive semiconductor. The bandgap of CdS is larger than that of a-Si, so OET made of CdS films are actuated using blue light (Higuchi et al., 2008). Functionality is also similar to the standard OET device, although a chemical process can be used for the CdS deposition, as opposed to PECVD for a-Si.

The OET device can also be reconfigured physically. One form is the use of amorphous-silicon-coated surfaces for both the upper and lower electrodes (Hwang et al., 2008b). This configuration is designed to reduce nonspecific particle adhesion when manipulation objects that experience negative OET forces, such as polystyrene beads. In the standard OET device, polystyrene beads can be levitated by the vertical component of the electric field gradient, bringing them into contact with the upper ITO-coated electrode. More than 50% of these particles adhere to the ITO-coated electrode, rendering them immovable by OET forces. By using a-Si for both electrodes, the forces due to the vertical electric field gradients are cancelled out, and the polystyrene beads remain at a metastable position that is approximately midway between the two electrode surfaces. In this version of the OET device, nonspecific adhesion is reduced to less than 20% of the particles (Hwang et al., 2008b). However, optical microscopy through the a-Si coated electrodes may present some viewing issues for certain types of particles, such as biological cells.

Another type of OET device combines the two discrete electrode surfaces onto a single substrate. This version of OET uses an interdigitated array of amorphous silicon electrodes to enable optical control of an electric field using a single substrate (Figure 3a). In this device, the electric field direction is primarily parallel to the surface of the substrate, so this configuration is known as lateral-field optoelectronic tweezers (LOET) (Ohta et al., 2007a) (Figure 3b). Using LOET, anisotropic particles such as microdisks (Tien et al., 2009) and nanowires (Ohta et al., 2007b; Ohta et al., 2008; Neale et al., 2009b) align with their long axis parallel to the surface of the LOET device, unlike in the conventional OET device (Jamshidi et al., 2008). In addition, the LOET device can be more easily integrated with other microdevices, as there is only one substrate.

Electrowetting-on-dielectric (EWOD) devices are an example of microsystems that can benefit from OET integration. EWOD devices can achieve complicated droplet-based manipulation (Cho et al., 2003; Srinivasan et al., 2004), but it is difficult to address objects within a droplet. OET functionality integrated with EWOD can create a platform capable of single-cell assays. In order to achieve OET integration with EWOD, an EWOD device and a LOET device were built on separate substrates, then sandwiched together to create a composite device that can perform droplet actuation as well as move cells within a droplet (Shah et al., 2009) (Figure 3c).

If the goal is droplet manipulation, another variant of the OET device can be used. The floating-electrode OET device is designed to manipulate aqueous droplets in oil for droplet-based assays (Park et al., 2008). In this device, electrodes are placed on top of an amorphous silicon layer, and the device is coated with a 15-μm-thick layer of polydimethylsiloxane (PDMS) polymer (Figure 3d). Optical patterns on the a-Si surface alter the applied electric field, producing a DEP force on the droplets suspended in oil. Movement of aqueous droplets was demonstrated at velocities of over 400 μm/s (Park et al., 2008).

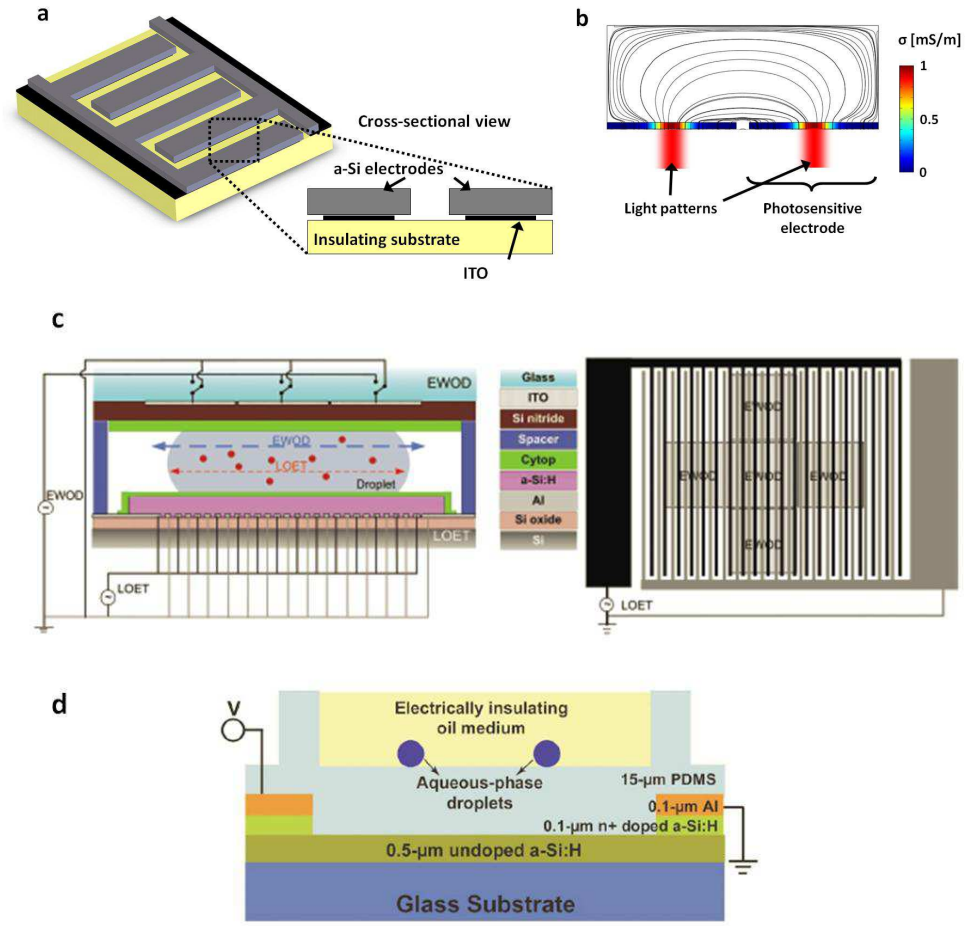

Fig. 3. Alternate OET configurations. (a) Lateral-field optoelectronic tweezers (LOET), which consist of an interdigitated array of a-Si electrodes. (b) Simulation of the electric field profile in the LOET device. The low-conductivity areas correspond to illuminated areas. (c) Integrated EWOD-LOET device for simultaneous droplet and cell manipulation. The LOET device is fabricated on the lower substrate, and the EWOD electrodes are fabricated on the upper substrate. Reprinted with permission from Shah et al., 2009. Copyright 2009, Royal Society of Chemistry. (d) Floating-electrode OET for the manipulation of droplets in oil. Reprinted with permission from Park et al., 2008. Copyright 2008, American Institute of Physics.

3. Cell manipulation using Optoelectronic Tweezers

3.1 Single-cell trapping

The most straightforward biological application of optoelectronic tweezers is for the trapping and transport of cells. OET trapping of many cell types using a variety of optical

patterns has been demonstrated, including *E. coli* bacteria (Chiou et al., 2004), red and white blood cells (Ohta et al., 2007c; Hwang et al., 2008a), HeLa cells (Ohta et al., 2007a; Neale et al., 2009a), Jurkat cells (Ohta et al., 2007a), yeast cells (Lu et al., 2005), and protozoa (Choi et al., 2008). One issue that arises when trapping mammalian cells is that of surface fouling, where cells nonspecifically adhere to the surface of OET devices. Cellular adhesion forces extend into the nanonewton range, whereas OET forces are typically tens to hundreds of piconewtons. Thus, once cells are fully adhered, it becomes difficult or impossible to actuate them by OET force.

In order to enable more reliable cellular trapping, OET devices were coated with a layer of poly(ethylene glycol) (PEG), a common antifouling polymer (Lau et al., 2009). The addition of the PEG coating resulted in 30 times less nonspecific adhesion as compared to uncoated OET devices, as tested with HeLa cells over the course of an hour. The PEG-coated devices allow reliable trapping and positioning of cells using OET manipulation. This was demonstrated by the formation of a 5 x 5 array of Jurkat cells on a PEG-coated OET device (Figure 3).

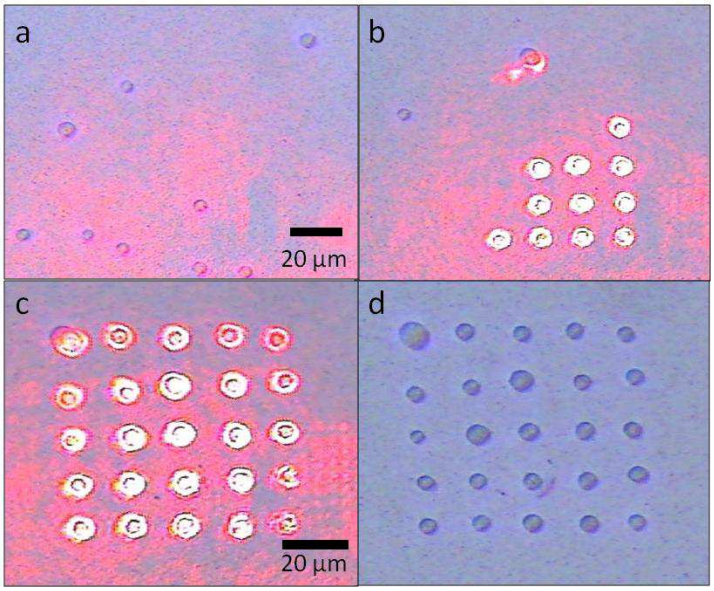

Fig. 3. Jurkat cell patterning on a PEG-coated OET device. (a) Initial random distribution of cells. (b) Formation of the array using OET manipulation. (c) Completed array. (d) Array with the optical manipulation pattern removed, for clarity. Reprinted with permission from Lau et al., 2009. Copyright 2009, Royal Society of Chemistry.

3.2 Cell separation

As described earlier, dielectrophoretic force is a function of the frequency-dependent electrical properties of the cells under manipulation. As different cell types exhibit dissimilar electrical properties, DEP can be used to sort between cell types, or even between widely varying cells of the same type (Gascoyne et al., 1997; Cheng et al., 1998; Huang et al., 2003; Gascoyne et al., 2004; Pethig et al., 2003). As OET uses DEP force, this capability can be used

to selectively concentrate live human B cells from dead B cells, and to spatially discriminate a mixed population of Jurkat and HeLa cells.

In a live cell, the semi-permeable cell membrane allows a cell to maintain an ion differential between its interior and the surrounding liquid medium. In these OET experiments, cells are suspended in a low-conductivity isotonic buffer (8.5% sucrose and 0.3% dextrose), so the cells have internal conductivities greater than the liquid. However, once a cell dies, this ion differential is no longer maintained, and the conductivity of the cell interior becomes similar to that of the surrounding liquid. Thus, the Clausius-Mossotti factor is different for live and dead cells, assuming that the internal permittivity and conductivity of a dead cell is equal to that of the surrounding media, while all other parameters remain the same as a live cell (Figure 4a). These simulated results predict that for applied frequencies greater than approximately 60 kHz, live B cells will experience a positive OET force, while dead B cells will experience a negative OET force.

The difference in DEP response between live and dead B cells is used to selectively concentrate live B cells at an applied frequency of 120 kHz (Chiou et al. 2005). The selective collection pattern is a series of broken concentric rings (Figure 4b). As the concentric rings shrink, the live cells are focused to the center of the pattern by positive OET. In contrast, the dead cells experience negative OET, and slip through the gaps in the ring patterns. Dead B cells are verified by adding 0.4% Trypan blue dye, which is excluded by the live cells, and absorbed by the dead cells. In these images, the live cells appear clear, and the dead cells appear dark.

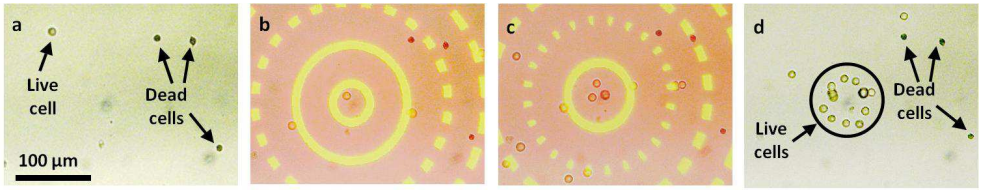

Fig. 4. Selective concentration of live and dead B cells. Reprinted with permission from Chiou et al., 2005. Copyright 2005, Nature Publishing Group.

OET force is also sensitive enough to distinguish between normal and abnormal live cells, which can improve the yield of *in vitro* fertilization procedures. This was demonstrated by the manipulation of oocytes cultured under standard condition and oocytes that had been kept in a nutrient-free solution for three days (Hwang et al., 2009b). By modelling oocytes using a protoplast structure, simulations predict that as cytoplasm conductivity decreases, the induced OET force also decreases. Hwang et al. hypothesize that this is the physical cause for different induced OET forces between the normal and nutrient-starved abnormal oocytes. It was observed that normal oocytes could be moved using OET patterns at approximately 12 µm/s, while the abnormal oocytes were unresponsive to OET manipulation (Hwang et al., 2009b).

In addition to differentiating between varying cells of the same type, OET force can be used to discriminate between different cell types. This ability is demonstrated through the spatial discrimination of live Jurkat and HeLa cells using OET.

In this experiment, cultured Jurkat cells were labeled with a green fluorescent dye. The labeled Jurkat cells and cultured HeLa cells are suspended in isotonic solution (Figure 5a). Culture media was added to adjust the conductivity of the cell solution to approximately 2

mS/m. Both cell types experience a positive OET force, and are attracted towards the optical manipulation patterns. However, the strength of the OET force varies according to the cell type, and also as a function of frequency (Ohta et al., 2007a). At an applied voltage of 10 Vpp at 100 kHz, sufficient variation in the OET force exists to differentiate between the two cell types using a scanning line optical pattern. A 15-μm-wide leading line and a 23-μm-wide trailing line are separated by ~40 μm, and are simultaneously scanned at a rate of 13 μm/s (Figure 5b). The leading line produces a weaker OET force than the thicker trailing line, as the manipulation velocity of cells exhibits a dependence on the width of the optical pattern (Ohta et al., 2007a; Ohta et al., 2007c). Thus, as the two lines are scanned across the OET device, the Jurkat cells, which experience a stronger OET force, are held by the leading line. The leading line does not produce sufficient force to transport the HeLa cells against the viscous drag, which are subsequently attracted to and transported by the trailing line. After the scan is completed, the cells retain a spatial separation equal to the spacing of the two scanning lines (Figure 5c). Fluorescent imaging is used to verify that the cells on the leading line pattern are the fluorescent-labeled Jurkat cells (Figure 5d).

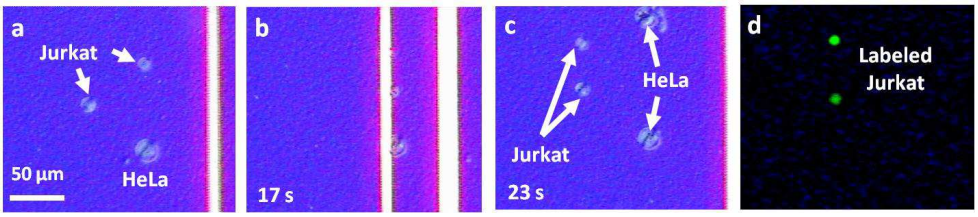

Fig. 5. Separation of live Jurkat and HeLa cells using OET. (a) Initial cell positions before the optical pattern is scanned from right to left across the field-of-view. (b) Cells are attracted to the leading line. The HeLa cell is starting to lag the scanning line. (c) Cells showing spatial separation after the scan is completed. An additional HeLa cell has moved into the field-of-view during the scan. (d) Fluorescent image of the cells in (c), verifying that the leading cells are the fluorescent-labeled Jurkat cells. The unlabeled HeLa cells do not appear in the fluorescent image. Reprinted with permissions from Ohta et al., 2007a. Copyright 2007, IEEE.

3.3 Light-induced electroporation

Other electric-field induced cellular operations can also be performed by the OET device. This includes electroporation, where electric pulses are used to temporarily open pores in the cellular membrane, allowing the introduction of molecules into cells. Currently, electroporation can be performed in a bulk procedure (Neumann et al., 1982) on thousands or millions of cells, restricting selectivity, or at the individual cell level (Lundqvistet al., 1998), in a time- and labor-intensive procedure. Although microfabricated devices have the potential to achieve electroporation at the single-cell level, with increased throughput (He et al., 2007; Khine et al., 2007; MacQueen et al., 2008; Yamada et al., 2008; Adamo & Jensen, 2008), this goal has not yet been achieved.

The OET device can be utilized as a platform to perform selective individual cell electroporation in parallel (Valley et al., 2009). The OET functionality allows single-cell resolution and selectivity of any cell within the OET manipulation area. In addition, the

electroporation can be performed in parallel, increasing throughput as compared to other single-cell electroporation techniques.

The parallel selective electroporation of HeLa cells was demonstrated using Propidium Iodide (PI) dye (Valley et al., 2009). The PI dye is normally membrane-impermeable. However, in the prescence of nucleic acids, the dye fluoresces red. Thus, a red fluorescent signal is evidence that cells have been successful electroporated, introducing PI dye into the cellular interior. Initially, OET manipulation is used to position the cells to be electroporated (Figure 6). Following this, two cells in the array corners are selectively illuminated by OET patterns, creating high electric field regions. An electroporation bias is briefly applied (1.5 kV/cm at 100 kHz for 5 s), electroporating only the illumated cells. This is verified by fluorescent microscopy, where only the illuminated cells show uptake and expression of the PI dye. A subsequent selective electroporation is performed to electroporate the remaining cells.

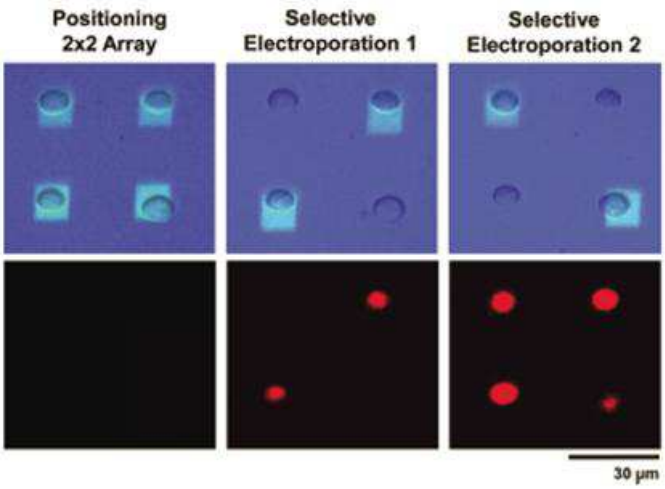

Fig. 6. Light-induced electroporation. Top row: Bright field microscopy of cells and optical patterns. Bottom row: Fluorescent microscopy showing PI dye. First, cells are arrayed using OET, which does not cause electroporation. Two cells on the diagonal are illuminated under the electroporation bias conditions (1.5 kV/cm). These cells fluoresce after uptaking PI dye (image taken 5 minutes following electroporation). Finally, the remaining two cells are electroporated, resulting in the fluorescence of all cells (image taken 5 minutes following electroporation). Reprinted with permission from Valley et al., 2009. Copyright 2009, Royal Society of Chemistry.

4. Micro- and nanoparticle assembly using Optoelectronic Tweezers

Optoelectronic tweezers is capable of assembling semiconducting and metallic micro- and nanoparticles for the creation of electronic and optoelectronic devices. This is demonstrated by the assembly of III-V semiconductor microdisk lasers on silicon for the integration of optical interconnects with CMOS circuits, and the assembly of semiconducting and metallic nanowires for nanowire-based devices.

4.1 Microdisk laser assembly on silicon

As the data transfer rates in computers increase, optical interconnects become attractive replacements for copper wiring. Silicon photonics provides an inexpensive method of integrating of CMOS electronics and optoelectronic components such as modulators and photodetectors for optical interconnects. However, on-chip optical sources are needed for most applications, necessitating the integration of semiconductor lasers with CMOS circuits on a silicon wafer. Silicon Raman lasers have been demonstrated (Boyraz & Jalali, 2004; Rong et al., 2005), but these require external optical pumps. Electrically-pumped lasers are only possible with compound semiconductor materials. Heteroepitaxy can grow compound semiconductor lasers directly on Si, but the growth temperature (> 400 °C) is usually too high for post-CMOS processing (Balakrishnan et al., 2006). To circumvent this issue, low temperature (300 °C) wafer bonding techniques have been used to integrate compound lasers on silicon wafers (Fang et al., 2006; Van Campenhout et al., 2007). However, integrating lasers on fully-processed CMOS wafers presents additional challenges as the silicon bonding surfaces are buried underneath up to ten layers of electrical interconnects. One approach is to build electrical interconnects and photonic circuits on separate Si wafers, bond the Si wafers, and then use flip-chip bonding to secure the III-V semiconductor materials on the Si wafers (Hattori et al., 2006). Another method to avoid any wafer bonding steps and enable simultaneous heterogeneous integration is an post-CMOS, optofluidic assembly process using LOET.

As the major axis of an anisotropic particle such as a microdisk aligns with the electric field lines, LOET must used to place the microdisks parallel to the surface of the device (standard OET would cause the disks to align with the major axis perpendicular to the OET surface). The microdisks used for the creation of on-chip lasers consist of an InGaAs/InGaAsP multiple-quantum-well structure, sandwiched by two larger-bandgap optical confinement layers, for a total thickness of 0.2 μm. Microdisks with diameters of 5 and 10 μm are fabricated from an InP epitaxial wafer, and suspended in ethanol for assembly by LOET.

The LOET electrodes create an optically-induced dielectrophoretic force, which is controlled by voltage applied across the electrodes and the position of optical patterns on the light-sensitive a-Si layer (Ohta et al., 2007a). The highest forces are in the illuminated areas near the electrode edges. Microdisks in solution are attracted to illuminated areas, and self-align in the gap between the electrodes (Figure 7). The optical patterns allow transportation of the microdisks along the length of the electrodes using an applied AC voltage of 1 to 10 Vpp at 200 kHz. Once the disks are aligned over a pedestal, the applied voltage is increased to 20 Vpp to hold the disks in place as the solution dries (Figure 7b, e). Ethanol is used to minimize surface tension forces during drying. After drying, the a-Si layer is removed by XeF_2 etching at 40 °C, so that the a-Si does not interfere with the optical mode of the microdisk. Subsequent SEM images show that the disks are aligned with an accuracy of approximately ± 0.25 μm (Figure 7c,f). This can be further improved by optimizing the optical imaging system.

Optical pumping of the assembled microdisk lasers show that at room temperature the 5- and 10-μm-diameter microdisks achieve single-mode lasing at wavelengths of 1558.7 nm and 1586 nm, at effective threshold pump powers of 0.34 mW and 1.0 mW, respectively (Tien et al., 2009). The threshold power for microdisks on the native InP wafer are similar to the threshold power of the assembled microdisks, indicating that the assembly process does not damage the disks.

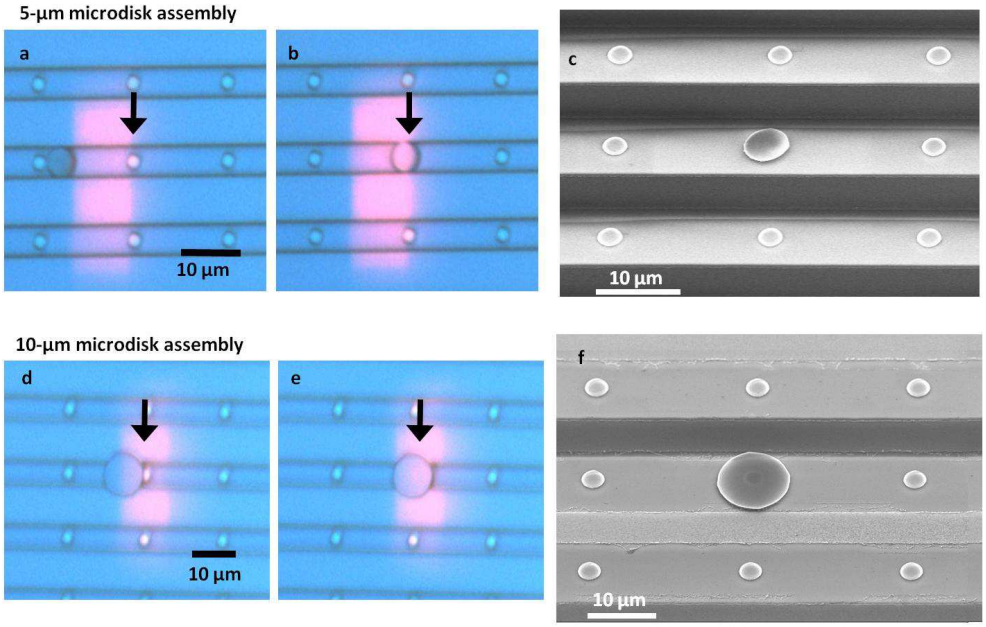

Fig. 7. III-V microdisk assembly. Assembly of a 5-µm-diameter microdisk (a, b) and a 10-µm-diameter microdisk (d, e) onto silicon pedestals. The target pedestals are indicated by arrows. (c, f) SEM images of the assembled microdisks.

4.2 Nanoparticle manipulation and assembly

Optoelectronic tweezers trapping works well for micron-scale objects, but the forces generated with OET typically are overcome by thermal (Brownian) fluctuations when particles are much smaller than 1 µm, as DEP force scales with r^3 (Equation 2). However, OET trapping is still possible when two dimensions of the particle are less than 100 nm, as long as the third dimension is on the order of micrometers. This anisotropy strengthens the particle dipole, increasing the DEP force. This effect is further enhanced for materials that are more polarizable than the liquid media, such as semiconductors or metals. As a result, OET is capable of exerting strong trapping forces both semiconducting and metallic nanowires with diameters as small as 20 nm (Jamshidi et al., 2008).

Nanowires experience a torque in addition to the DEP force, which aligns the long-axis of the nanowire with the electric field in the OET device. Therefore, the nanowire is aligned normal to the photoconductive electrode surface of the OET device. (If necessary, LOET can be used to manipulate nanowires parallel to the surface of the OET device [Ohta et al., 2007b; Ohta et al., 2008; Neale et al., 2009b]).

Once a nanowire is contained in an OET trap, the Brownian motion is significantly reduced. Without OET trapping, the nanowire covers an area of 28.9 μm^2; while in the OET trap, the nanowire is localized to an area of 0.22 μm^2, corresponding to a trap stiffness of 0.16 pN/µm (Jamshidi et al., 2008). Normalizing trap stiffness with respect to optical power results in 1.6×10^{-6} N/(m×mW), which is approximately 2 orders of magnitude larger than for an optical tweezers nanowire trap (Jamshidi et al., 2008). Maximum trapping speeds for an

individual silicon nanowire with 100 nm diameter and 5 μm length approach 135 μm/s with a peak-to-peak trapping voltage of 20V, which is approximately 4 times the maximum speed achievable by optical tweezers (Pauzauskie et al., 2006) and is reached with 5-6 orders of magnitude less optical power density than optical tweezers.

In addition to the trapping of single nanowires, OET can be used to perform the parallel assembly of nanowires using real-time dynamic trapping. The formation of an individually-addressable 5×5 array of single silver nanowires has been demonstrated (Figure 8a). In addition, large-scale arrays of nanowires can be formed using appropriate optical patterns. The density of the trapped silver nanowires can also be tuned by varying the size of a rectangular trapping pattern in real-time (Figure 8b). The trapping density is ultimately limited by the strength of the dipole-dipole interactions between the nanowires.

Once the nanowires have been trapped, it is possible to preserve the position and orientation of the wires trapped with OET using a photocurable polymer solution such as PEGDA, enabling immobilization of nanowires in the polymer matrix within seconds by exposing the manipulation area to an ultra-violet source (Jamshidi et al., 2008). The ability to preserve the position and orientation of OET-trapped nanowires enables subsequent post-processing steps.

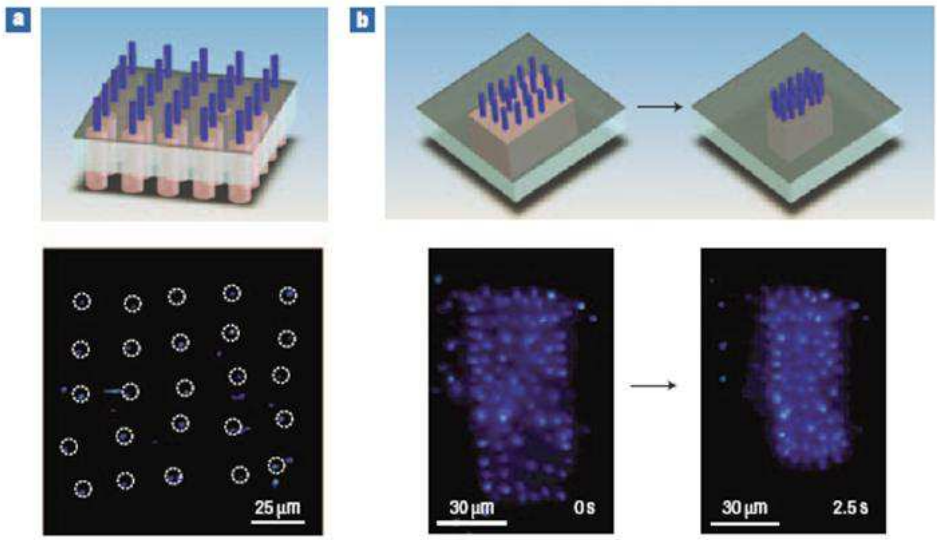

Fig. 8. Nanowire manipulation using OET. (a) Positioning silver nanowires into a 5 x 5 array. The top image shows a conceptual diagram; the bottom images show the microscope image, with the trapped nanowires circled for clarity. (b) Control of nanowire density by adjusting the size of the trapping pattern. More than 80 silver nanowires are concentrated from an area of approximately 3,000 μm² to 2,000 μm². Reprinted with permission from Jamshidi et al., 2008. Copyright 2008, Nature Publishing Group.

5. Future directions

New versions of the OET device are being developed. One promising device promises to improve OET manipulation of live cells. Currently, efficient OET operation requires cells to

be suspended in a low-conductivity, isotonic media. This is beneficial for separating live and dead cells, as it results in OET forces of opposing polarities. However, isotonic media is not ideal for long-term cell viability or for fragile cells. In these cases, it is desirable to manipulate cells in their nature culture media. Unfortunately, typical cell culture media contains high concentrations of ions, resulting in an inefficient switching between the "on" and "off" states of the optically-defined OET electrodes. In order to observe OET actuation, prohibitively high optical intensities must be used.

One way to improve OET operation in high-conductivity cell culture media is to improve the illuminated photoconductivity of the OET device. This can be accomplished by replacing the a-Si material with a single-crystal silicon phototransistor structure. This phototransistor-based OET device (Ph-OET) manages to enhance the photoconductive response by more than 2 orders of magnitude as compared to a-Si, enabling OET operation in cell culture media (Hsu et al., 2009). The Ph-OET device provides more than 2 orders of magnitude of photoconductivity compared to a-Si under same illumination and bias, thanks to the high phototransistor gain and the high electron mobility of single crystalline silicon. The Ph-OET device can be actuated with an optical intensity of 1 W/cm^2. At these optical intensities, a-Si-based OET devices can only be actuated in low-conductivity media. Thus, the Ph-OET device promises to enable new applications of OET manipulation on live cells.

6. Summary

Optoelectronic tweezers and its variants are versatile devices for the manipulation of microparticles, nanoparticles, and cells. This chapter presented the theory and operation of the OET device and its variants, along with descriptions of various applications, including cell trapping and sorting, cell electroporation, microdisk laser assembly, and nanoparticle manipulation and assembly. Currently, the most promising fields for applications are biological research and micro- and nanoassembly. However, as OET is a relatively new tool, more applications are being developed that take advantage of the many capabilities of OET.

7. References

Adamo A. & Jensen, K. F. (2008). Microfluidic based single cell microinjection. *Lab on a Chip*, vol. 8, no. 8, 1258–1261.

Ashkin, A.; Dziedzic, J. M.; Bjorkholm, J. E. & Chu, S. (1986). Observation of a single-beam gradient force optical trap for dielectric particles. *Optics Letters*, vol. 11, no. 5, 288-290.

Avouris, P.; Hertel, T.; Martel, R.; Schmidt, T.; Shea, H. R. & Walkup, R. E. (1999). Carbon nanotubes: nanomechanics, manipulation, and electronic devices. *Applied Surface Science*, vol. 141, no. 3-4, 201-209.

Balakrishnan, G.; Jallipalli, A.; Rotella, P.; Huang, S.; Khoshakhlagh, A.; Amtout, A.; Krishna, S.; Dawson, L. R. & Huffaker, D. L. (2006). Room-temperature optically pumped (Al)GaSb vertical-cavity surface-emitting laser monolithically grown on an Si(100) substrate. *IEEE Journal of Selected Topics in Quantum Electronics*, vol. 12, no. 6, 1636-1641.

Boyraz O. & Jalali, B. (2004). Demonstration of a silicon Raman laser. *Optics Express*, vol. 12, no. 21, 5269-5273.

Cheng, J.; Sheldon, E. L.; Wu, L.; Heller, M. J. & O'Connell, J. P. (1998). Isolation of cultured cervical carcinoma cells mixed with peripheral blood cells on a bioelectronic chip. *Analytical Chemistry*, vol. 70, no. 11, 2321-2326.

Chiou, P. Y.; Wong, W.; Liao, J. C. & Wu, M. C. (2004). Cell addressing and trapping using novel optoelectronic tweezers, in *Proceedings of the 17th IEEE International Conference on Micro Electro Mechanical Systems (MEMS)*, pp. 21-24, Maastricht, Netherlands.

Chiou, P. Y.; Ohta, A. T. & Wu, M. C. (2005). Massively parallel manipulation of single cells and microparticles using optical images. *Nature*, vol. 436, no. 7049, 370-372.

Chiou, P. Y.; Ohta, A. T.; Jamshidi, A.; Hsu, H. Y. & Wu, M. C. (2008). Light-actuated ac electroosmosis for nanoparticle manipulation. *Journal of Microelectromechanical Systems*, vol. 17, no. 3, 525-531.

Cho, S. K.; Moon H. J. & Kim, C.-J. (2003). Creating, transporting, cutting, and merging liquid droplets by electrowetting-based actuation for digital microfluidic circuits. *Journal of Microelectromechanical Systems*, vol. 12, no. 1, pp. 70–80.

Choi, W.; Kim, S. H.; Jang, J. & Park, J. K. (2007). Lab-on-a-display: a new microparticle manipulation platform using a liquid crystal display (LCD). *Microfluidics and Nanofluidics*, vol. 3, no. 2, 217-225.

Choi, W.; Nam, S. W.; Hwang, H.; Park, S. & Park, J. K. (2008). Programmable manipulation of motile cells in optoelectronic tweezers using a grayscale image. *Applied Physics Letters*, vol. 93, no. 14, 143901-3.

Chronis, N. & Lee, L. P. (2005). Electrothermally activated SU-8 microgripper for single cell manipulation in solution. *Journal of Microelectromechanical Systems*, vol. 14, no. 4, 857-863.

Evoy, S.; DiLello, N.; Deshpande, V.; Narayanan, A.; Liu, H.; Riegelman, M.; Martin, B. R.; Hailer, B.; Bradley, J.-C.; Weiss, W.; Mayer, T. S.; Gogotsi, Y.; Bau, H. H.; Mallouk, T. E. & Raman, S. (2004). Dielectrophoretic assembly and integration of nanowire devices with functional CMOS operating circuitry. *Microelectronic Engineering*, vol. 75, no. 1, 31-42.

Fang, A. W.; Park, H.; Cohen, O.; Jones, R.; Paniccia, M. J. & Bowers, J. E. (2006). Electrically pumped hybrid AlGaInAs-silicon evanescent laser. *Optics Express*, vol. 14, no. 20, 9203-9210.

Fuchs, A. B.; Romani, A.; Freida, D.; Medoro, G.; Abonnenc, M.; Altomare, L.; Chartier, I.; Guergour, D.; Villiers, C.; Marche, P. N.; Tartagni, M.; Guerrieri, R.; Chatelain, F. & Manaresi, N. (2006). Electronic sorting and recovery of single live cells from microlitre sized samples. *Lab on a Chip*, vol. 6, no. 1, 121-126.

Garces-Chavez, V.; Dholakia, K. & Spalding, G. C. (2005). Extended-area optically induced organization of microparticies on a surface. *Applied Physics Letters*, vol. 86, no. 3, 031106-3.

Gascoyne, P. R. C.; Wang, X.-B.; Huang, Y. & Becker, F. F. (1997). Dielectrophoretic separation of cancer cells from blood. *IEEE Transactions on Industry Applications*, vol. 33, no. 3, 670-8.

Gascoyne, P. R. C. & Vykoukal, J. V. (2004). Dielectrophoresis-based sample handling in general-purpose programmable diagnostic instruments. *Proceedings of the IEEE*, vol. 92, no. 1, 22-42.

Grigorenko, A. N.; Roberts, N. W.; Dickinson, M. R. & Zhang, Y. (2008). Nanometric optical tweezers based on nanostructured substrates. *Nature Photonics*, vol. 2, no. 6, 365-370.

Gosse, C. & Croquette, V. (2002). Magnetic tweezers: Micromanipulation and force measurement at the molecular level. *Biophysical Journal*, vol. 82, no. 6, 3314-3329.

Grier, D. G. (2003). A revolution in optical manipulation. *Nature*, vol. 424, no. 6950, 810-816.

Hattori, H. T.; Seassal, C.; Touraille, E.; Rojo-Romeo, P.; Letartre, X.; Hollinger, G.; Viktorovitch, P.; Di Cioccio, L.; Zussy, M.; Melhaoui, L. E. & Fedeli, J. M. (2006). Heterogeneous integration of microdisk lasers on silicon strip waveguides for optical interconnects. *IEEE Photonics Technology Letters*, vol. 18, no. 1, 223-225.

He, H. Q.; Chang D. C. & Lee, Y. K. (2007). Using a micro electroporation chip to determine the optimal physical parameters in the uptake of biomolecules in HeLa cells. *Bioelectrochemistry*, vol. 70, 363–368.

Higuchi, Y.; Kusakabe, T.; Tanemura, T.; Sugano, K.; Tsuchiya, T. & Tabata, O. (2008). Manipulation system for nano/micro components integration via transportation and self-assembly, in *Proceedings of the IEEE 21st International Conference on Micro Electro Mechanical Systems (MEMS)*, pp. 836-839, Tucson, AZ, USA.

Hsu, H.-Y.; Ohta, A. T.; Chiou, P.-Y.; Jamshidi, A.; Neale, S. & Wu, M. C. (2009). Phototransistor-based optoelectronic tweezers for dynamic cell manipulation in cell culture media. *Lab on a Chip*, DOI: 10.1039/b906593h.

Huang, Y.; Yang, J. M.; Hopkins, P. J.; Kassegne, S.; Tirado, M.; Forster, A. H. & Reese, H. (2003). Separation of simulants of biological warfare agents from blood by a miniaturized dielectrophoresis device. *Biomedical Microdevices*, vol. 5, no. 3, 217-225.

Hwang, H.; Choi, Y. J.; Choi, W.; Kim, S. H.; Jang, J. & Park, J. K. (2008a). Interactive manipulation of blood cells using a lens-integrated liquid crystal display based optoelectronic tweezers system. *Electrophoresis*, vol. 29, no. 6, 1203-1212.

Hwang, H.; Oh, Y.; Kim, J. J.; Choi, W.; Park, J. K.; Kim, S. H. & Jang, J. (2008b). Reduction of nonspecific surface-particle interactions in optoelectronic tweezers. *Applied Physics Letters*, vol. 92, no. 2, 024108-3.

Hwang, H. & Park, J. K. (2009a). Rapid and selective concentration of microparticles in an optoelectrofluidic platform. *Lab on a Chip*, vol. 9, no. 2, 199-206.

Hwang, H.; Lee, D. H.; Choi, W. & Park, J. K. (2009b). Enhanced discrimination of normal oocytes using optically induced pulling-up dielectrophoretic force. *Biomicrofluidics*, vol. 3, no. 1, 014103-10.

Jamshidi, A.; Pauzauskie, P. J.; Schuck, P. J.; Ohta, A. T.; Chiou, P. Y.; Chou, J.; Yang, P. & Wu, M. C. (2008). Dynamic manipulation and separation of individual semiconducting and metallic nanowires. *Nature Photonics*, vol. 2, no. 2, 85-89.

Jones, T. B. *Electromechanics of Particles*. Cambridge: Cambridge University Press, 1995.

Khine, M.; Ionescu-Zanetti, C.; Blatz, A.; Wang L. P. & Lee, L. P. (2007). Single-cell electroporation arrays with real-time monitoring and feedback control. *Lab on a Chip*, vol. 7, no. 4, 457–462.

Kim, C.-J.; Pisano, A. P. & Muller, R. S. Silicon-Processed Overhanging Microgripper. *Journal of Microelectromechanical Systems*, vol. 1, no. 1, pp. 31-36.

Konig, K.; Liang, H.; Berns, M. W. & Tromberg, B. J. (1996). Cell damage in near-infrared multimode optical traps as a result of multiphoton absorption. *Optics* Letters, vol. 21, no. 14, 1090-1092.

Krupke, R.; Hennrich, F.; von Lohneysen, H. & Kappes, M. M. (2003). Separation of metallic from semiconducting single-walled carbon nanotubes. *Science*, vol. 301, no. 5631, 344-347.

Lau, A. N. K.; Ohta, A. T.; Phan, H. L.; Hsu, H.-Y.; Jamshidi, A.; Chiou, P.-Y. & Wu, M. C. (2009). Antifouling coatings for optoelectronic tweezers. *Lab on a Chip*, DOI: 10.1039/B907840A.

Lu, Y.-S.; Huang, Y.-P.; Yeh, J. A.; Lee, C. & Chang, Y.-H. (2005). Controllability of non-contact cell manipulation by image dielectrophoresis (iDEP). *Optical and Quantum Electronics*, vol. 37, no. 13-15, 1385-1395.

Lundqvist, J. A.; Sahlin, F. ; Aberg, M. A. I. ; Stromberg, A.; Eriksson, P. S. & Orwar, O. (1998). Altering the biochemical state of individual cultured cells and organelles with ultramicroelectrodes. *Proceedings of the National Academy of Sciences of the United States of America*, vol. 95, no. 18, 10356–10360.

MacDonald, M. P.; Spalding, G. C. & Dholakia, K. (2003). Microfluidic sorting in an optical lattice," *Nature*, vol. 426, no. 6965, 421-424.

MacQueen, L. A.; Buschmann M. D. & Wertheimer, M. R. (2008). Gene delivery by electroporation after dielectrophoretic positioning of cells in a non-uniform electric field. *Bioelectrochemistry*, vol. 72, no. 2, 141–148.

Maier, B.; Koomey, M. & Sheetz, M. P. (2004). A force-dependent switch reverses type IV pilus retraction. *Proceedings of the National Academy of Sciences of the United States of America*, vol. 101, no. 30, 10961-10966.

Miao, X. & Lin, L. Y. (2007). Trapping and manipulation of biological particles through a plasmonic platform. *IEEE Journal of Selected Topics in Quantum Electronics*, vol. 13, no. 6, 1655-1662.

Mohanty, S. K.; Rapp, A.; Monajembashi, S.; Gupta, P. K. & Greulich, K. O. (2002). Comet assay measurements of DNA damage in cells by laser microbeams and trapping beams with wavelengths spanning a range of 308 nm to 1064 nm. *Radiation Research*, vol. 157, no. 4, 378-385.

Muller, T.; Gerardino, A.; Schnelle, T.; Shirley, S. G.; Bordoni, F.; Gasperis, G. D.; Leoni, R. & Fuhr, G. (1996). Trapping of micrometre and sub-micrometre particles by high-frequency electric fields and hydrodynamic forces. *Journal of Physics D-Applied Physics*, vol. 29, no. 2, 340-349.

Neale, S. L.; Mazilu, M.; Wilson, J. I. B.; Dholakia, K. & Krauss, T. F. (2007). The resolution of optical traps created by light induced dielectrophoresis (LIDEP). *Optics Express*, vol. 15, no. 20, 12619-12626.

Neale, S. L.; Ohta, A. T.; Hsu, H.-Y.; Valley, J. K.; Jamshidi, A. & Wu, Ming C. (2009a). Trap profiles of projector based optoelectronic tweezers (OET) with HeLa cells. Optics Express, vol. 17, no. 7, 5232-5239.

Neale, S.L.; Fan, Z.; Ohta, A. T.; Jamshidi, A.; Valley, J. K.; Hsu, H.-Y.; Javey, A. & Wu, M. C. (2009b). Optofluidic assembly of red/blue/green semiconductor nanowires, in *Proceedings of the Conference on Lasers and Electro-Optics (CLEO)*, Baltimore, MD, USA.

Neuman, K. C.; Chadd, E. H.; Liou, G. F.; Bergman, K. & Block, S. M. (1999). Characterization of photodamage to Escherichia coli in optical traps. *Biophysical Journal*, vol. 77, no. 5, 2856-2863.

Neumann, E.; Schaeferridder, M.; Wang, Y. & Hofschneider, P. H. (1982). Gene transfer into mouse lyoma cells by electroporation in high electric fields. *The EMBO Journal*, vol. 1, no. 7, 841–845.

Ohta, A. T.; Chiou, P.-Y.; Phan, H. L.; Sherwood, S. W.; Yang, J. M.; Lau, A. N. K.; Hsu, H.-Y.; Jamshidi, A. & Wu, M. C. (2007a). Optically Controlled Cell Discrimination and Trapping Using Optoelectronic Tweezers. *IEEE Journal of Selected Topics in Quantum Electronics*, vol. 13, no. 2, 235-243.

Ohta, A. T.; Jamshidi, A.; Pauzauskie, P. J.; Hsu, H.-Y.; Yang, P. & Wu, M. C. (2007b). Trapping and transport of silicon nanowires using lateral-field optoelectronic tweezers, in *Proceedings of the Conference on Lasers and Electro-Optics (CLEO)*, pp. 828-829, Baltimore, MD, USA.

Ohta, A. T.; Chiou, P. Y.; Han, T. H.; Liao, J. C.; Bhardwaj, U.; McCabe, E. R. B.; Yu, F.; Sun, R. & Wu, M. C. (2007c) Dynamic Cell and Microparticle Control via Optoelectronic Tweezers. *Journal of Microelectromechanical Systems*, vol. 16, no. 3, 491-499.

Ohta, A. T.; Neale, S.L.; Hsu, H.-Y.; Valley, J. K. & Wu, M. C. (2008). Parallel assembly of nanowires using lateral-field optoelectronic tweezers, in *Proceedings of the IEEE/LEOS International Conference on Optical MEMs and Nanophotonics*, pp. 7-8, Freiburg, Germany.

Padinger, F.; Rittberger, R. S. & Sariciftci, N. S. (2003). Effects of Postproduction Treatment on Plastic Solar Cells. *Advanced Functional Materials*, vol. 13, no. 1, pp. 85-88.

Park, S.; Pan, C.; Wu, T.-H.; Kloss, C.; Kalim, S.; Callahan, C. E.; Teitell, M. & Chiou, E. P. Y. (2008). Floating electrode optoelectronic tweezers: light-driven dielectrophoretic droplet manipulation in electrically insulating oil medium. *Applied Physics Letters*, vol. 92, no. 15, 151101-1-3.

Paterson, L.; Papagiakoumou, E.; Milne, G.; Garces-Chavez, V.; Tatarkova, S. A.; Sibbett, W.; Gunn-Moore, F. J.; Bryant, P. E.; Riches, A. C. & Dholakia, K. (2005). Light-induced cell separation in a tailored optical landscape. *Applied Physics Letters*, vol. 87, no. 12, 123901-3.

Pauzauskie, P. J.; Radenovic, A.; Trepagnier, E.; Shroff, H.; Yang, P. & Liphardt, J. (2006). Optical trapping and integration of semiconductor nanowire assemblies in water. *Nature Materials*, vol. 5, no. 2, 97-101.

Pethig, R.; Talary, M. S. & Lee, R. S. (2003). Enhancing traveling-wave dielectrophoresis with signal superposition. *IEEE Engineering in Medicine and Biology Magazine*, vol. 22, no. 6, 43-50.

Pohl, H. A. (1958). Some Effects of Nonuniform Fields on Dielectrics. *Journal of Applied Physics*, vol. 29, no. 8, 1182-1188.

Rong, H. S.; Jones, R.; Liu, A.; Cohen, O.; Hak, D.; Fang A. & Paniccia, M. (2005). A continuous-wave Raman silicon laser. *Nature*, vol. 433, no. 7027, 725-728.

Shah, G. J.; Ohta, A. T.; Chiou, E. P. Y.; Wu, M. C. & Kim, C.-J. (2009). EWOD-driven droplet microfluidic device integrated with optoelectronic tweezers as an automated platform for cellular isolation and analysis. *Lab on a Chip*, vol. 9, no. 12, 1732-1739.

Srinivasan, V.; Pamula, V. K. & Fair, R. B. (2004). An integrated digital microfluidic lab-on-a-chip for clinical diagnostics on human physiological fluids. *Lab on a Chip*, vol. 4, no. 4, pp. 310–315.

Tien, M.-C.; Ohta, A. T.; Yu, K.; Neale, S. L. & Wu, M. C. (2009). Heterogeneous integration of InGaAsP microdisk laser on a silicon platform using optofluidic assembly. *Applied Physics A: Materials Science & Processing*, vol. 95, no. 4, 967-972.

Valley, J. K.; Jamshidi, A.; Ohta, A. T.; Hsu, H.-Y. & Wu, M. C. (2008). Operational regimes and physics present in optoelectronic tweezers. *Journal of Microelectromechanical Systems*, vol. 17, no. 2, 342-50.

Valley, J. K.; Neale, S.; Hsu, H.-Y.; Ohta, A. T.; Jamshidi, A. & Wu, M. C. (2009). Parallel single-cell light-induced electroporation and dielectrophoretic manipulation. *Lab on a Chip*, vol. 9, no. 12, pp. 1714-1720.

Van Campenhout, J.; Rojo-Romeo, P.; Regreny, P.; Seassal, C.; Van Thourhout, D.; Verstuyft, S.; Di Cioccio, L.; Fedeli, J.-M.; Lagahe, C. & Baets, R. (2007). Electrically pumped InP-based microdisk lasers integrated with a nanophotonic silicon-on-insulator waveguide circuit. *Optics Express*, vol. 15, no. 11, 6744-6749.

Wang, W.; Lin, L.-H.; Guo, T.-F. & Lee, G.-B. (2009). Manipulation of Biosamples and Microparticles using Optical Images on Polymer Devices, in *Proceedings of the IEEE 22nd International Conference on Micro Electro Mechanical Systems (MEMS)*, pp. 415-418, Sorrento, Italy.

West, J.; Becker, M.; Tombrink, S. & Manz, A. (2008). Micro total analysis systems: Latest achievements. *Analytical Chemistry*, vol. 80, no. 12, 4403-4419.

Yamada, M.; Kobayashi, J.; Yamato, M.; Seki M. & Okano, T. (2008). Millisecond treatment of cells using microfluidic devices via two-step carrier-medium exchange. *Lab on a Chip*, vol. 8, no. 5, 772–778.

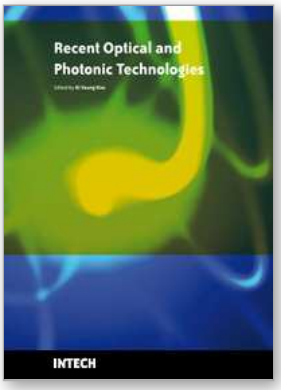

Recent Optical and Photonic Technologies

Edited by Ki Young Kim

ISBN 978-953-7619-71-8
Hard cover, 450 pages
Publisher InTech
Published online 01, January, 2010
Published in print edition January, 2010

Research and development in modern optical and photonic technologies have witnessed quite fast growing advancements in various fundamental and application areas due to availability of novel fabrication and measurement techniques, advanced numerical simulation tools and methods, as well as due to the increasing practical demands. The recent advancements have also been accompanied by the appearance of various interdisciplinary topics. The book attempts to put together state-of-the-art research and development in optical and photonic technologies. It consists of 21 chapters that focus on interesting four topics of photonic crystals (first 5 chapters), THz techniques and applications (next 7 chapters), nanoscale optical techniques and applications (next 5 chapters), and optical trapping and manipulation (last 4 chapters), in which a fundamental theory, numerical simulation techniques, measurement techniques and methods, and various application examples are considered. This book deals with recent and advanced research results and comprehensive reviews on optical and photonic technologies covering the aforementioned topics. I believe that the advanced techniques and research described here may also be applicable to other contemporary research areas in optical and photonic technologies. Thus, I hope the readers will be inspired to start or to improve further their own research and technologies and to expand potential applications. I would like to express my sincere gratitude to all the authors for their outstanding contributions to this book.

How to reference

In order to correctly reference this scholarly work, feel free to copy and paste the following:

Aaron T. Ohta, Pei-Yu Chiou, Arash Jamshidi, Hsan-Yin Hsu, Justin K. Valley, Steven L. Neale, and Ming C. Wu (2010). Optoelectronic Tweezers for the Manipulation of Cells, Microparticles, and Nanoparticles, Recent Optical and Photonic Technologies, Ki Young Kim (Ed.), ISBN: 978-953-7619-71-8, InTech, Available from: http://www.intechopen.com/books/recent-optical-and-photonic-technologies/optoelectronic-tweezers-for-the-manipulation-of-cells-microparticles-and-nanoparticles

INTECH
open science | open minds

InTech Europe
University Campus STeP Ri
Slavka Krautzeka 83/A
51000 Rijeka, Croatia
Phone: +385 (51) 770 447

InTech China
Unit 405, Office Block, Hotel Equatorial Shanghai
No.65, Yan An Road (West), Shanghai, 200040, China
中国上海市延安西路65号上海国际贵都大饭店办公楼405单元
Phone: +86-21-62489820

Fax: +385 (51) 686 166
www.intechopen.com

Fax: +86-21-62489821